PNAS
www.pnas.org

Supplementary Information for

Phasor histone FLIM-FRET microscopy quantifies spatiotemporal rearrangement of chromatin architecture during the DNA damage response.

Jieqiong Lou[a,1], Lorenzo Scipioni[b,1], Belinda K. Wright[c], Tara K. Bartolec[d], Jessie Zhang[d], V. Pragathi Masamsetti[d], Katharina Gaus[c,e], Enrico Gratton[b], Anthony J. Cesare[d,2], Elizabeth Hinde[a,c,e,2].

Anthony J. Cesare
Email: tcesare@cmri.org.au,

Elizabeth Hinde
Email: elizabeth.hinde@unimelb.edu.au

This PDF file includes:

Supplementary Text
Figs. S1 to S10
Table S1

www.pnas.org/cgi/doi/10.1073/pnas.1814965116

Supplementary Information Text

1. Phasor Transformation

Phasor transformation and data analysis were performed in SimFCS. The decay *I(t)* in each pixel of a FLIM image is transformed into its sine and cosine components which are then represented in a two-dimensional polar plot (phasor plot), according to:

$$g_{i,j}(\omega) = \frac{\int_0^\infty I_{i,j}(t)cos(\omega t)dt}{\int_0^\infty I_{i,j}(t)dt} \quad (1)$$

$$s_{i,j}(\omega) = \frac{\int_0^\infty I_{i,j}(t)sin(\omega t)dt}{\int_0^\infty I_{i,j}(t)dt} \quad (2)$$

where ω is the laser repetition angular frequency (2πf) and the indexes *i* and *j* identify a pixel of the image. If the decay is single exponential $I(t) = Ae^{-\frac{t}{\tau}}$ the coordinates of the phasor are given by:

$$g_{i,j}(\omega) = \frac{1}{1+(\omega\tau)^2} \quad (3)$$

$$s_{i,j}(\omega) = \frac{\omega\tau}{1+(\omega\tau)^2} \quad (4)$$

In the case where a pixel *i, j* has the contribution of several exponential components, the coordinates g and s of the phasor are given by:

$$g_{i,j}(\omega) = \sum_k \frac{f_k}{1+(\omega\tau_k)^2} \quad (5)$$

$$s_{i,j}(\omega) = \sum_k \frac{f_k\omega\tau_k}{1+(\omega\tau_k)^2} \quad (6)$$

where f_k is the intensity weighted fractional contribution of the component with lifetime τ_k. According to expressions 3 and 4 the coordinates of a phasor for a single exponential decay are $s_{i,j}^2 + \left(g_{i,j} - \frac{1}{2}\right)^2 = \frac{1}{4}$, which implies that all single exponential components are represented by a semi-circle of center $\left(\frac{1}{2}, 0\right)$ and radius $\frac{1}{2}$ in the phasor plot. We name this the "universal circle'. Along this semicircle a phasor corresponding to a very short lifetime (small phase angle) is close to the point (1,0), where as a phasor corresponding to a very long lifetime will be close to the (0,0) point.

2. Resolution of two components

To resolve the fractional contribution of two phasor components we graphically solve equations 5 and 6 in the phasor plot. All phasors corresponding to the combination of the component phasors are along a segment where the segment extremes correspond to the phasors of the two isolated components. Generally, the locations of the two component phasors are known or are derived from independent measurement. The segment is drawn on the phasor plot and the operator selects points along the segment to match the experimental points. The fractional contribution of the two phasors at the cursor location is displayed on the screen. Using the reciprocal property of the cursor, the points in the image corresponding to that particular solution are highlighted.

3. FRET efficiency calculation

The FRET trajectory is calculated according to the classical definition of FRET efficiency:

$$E = 1 - \frac{\tau}{\tau_D} \qquad (7)$$

The phasor of the donor in the absence of the acceptor τ_D is obtained from an independent preparation in which the acceptor is absent. The phasor corresponding to the quenched donor is calculated according to equation 7. The realization of all possible phasors that are quenched with different efficiencies describe a curved trajectory in the phasor plot. The experimental position of the phasor of a given pixel along the trajectory determines the amount of quenching and therefore the FRET efficiency. The contributions of the background and of the donor without acceptor are evaluated using the rule of the linear combination (equations 5 and 6), with the background phasor also determined independently. The operator moves the cursor along the curved trajectory to the point where there is a cluster of phasors. Using the reciprocal property of the cursor, the pixels in the image corresponding to a given FRET efficiency are highlighted.

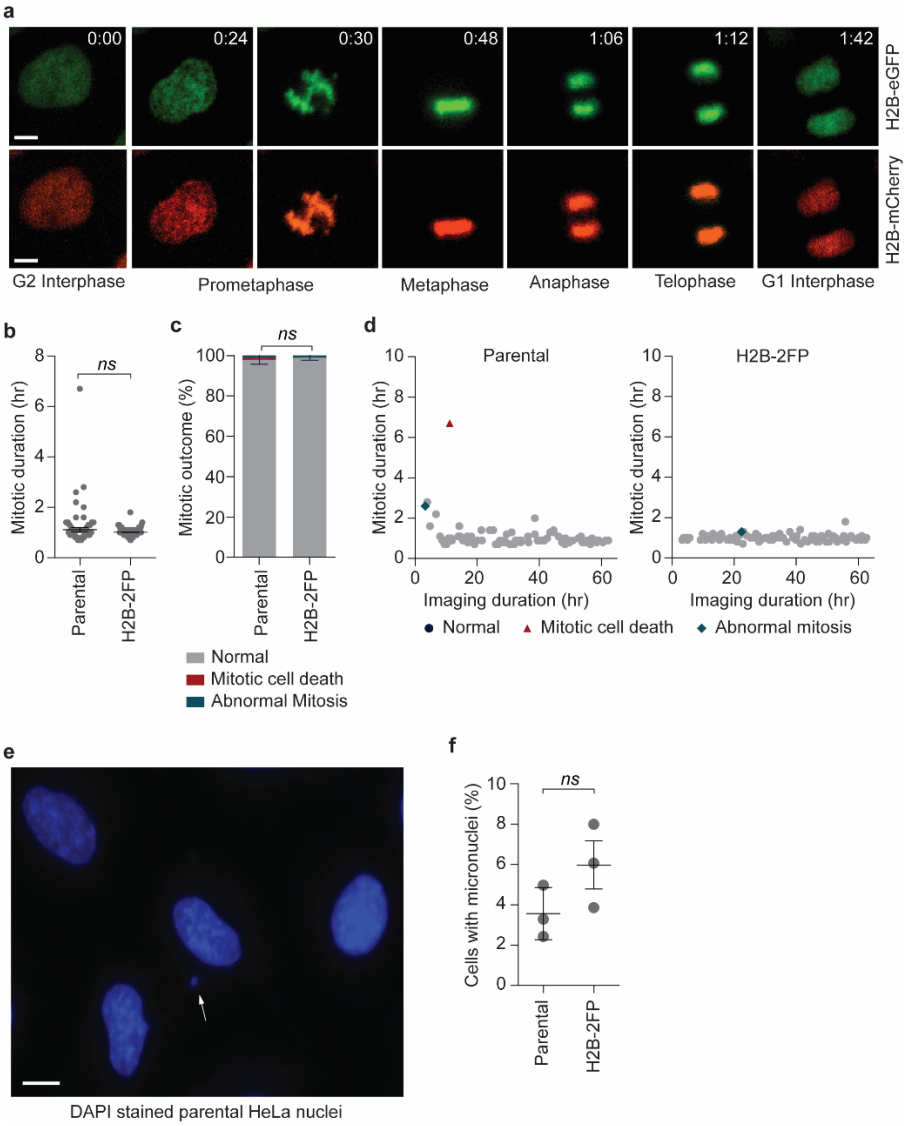

Figure S1: HeLa$^{H2B\text{-}2FP}$ verification and assessment of genome stability. (a) Incorporation of H2B-eGFP and H2B-mCherry into chromatin was verified by live cell imaging of HeLa$^{H2B\text{-}2FP}$ passing through mitosis. (b-d) Mitotic phenotypes were measured in HeLa parental vs HeLa$^{H2B\text{-}2FP}$ cells as a measure of genome stability. Mitotic duration (b) and outcome (c) were not impacted by exogenous histone expression in HeLa$^{H2B\text{-}2FP}$ [n = 2 biological replicates of ≥ 40 mitoses per replicate, grouped into a single Tukey Box plot (b), or shown as a histogram mean ± range (c). *ns* = not significant, Mann-Whitney Text (b), Fisher Exact Test (c)]. (d) Two-dimensional plots of the data from (b, c). Each point represents a mitotic event. Location of a symbol relative to the x-axis indicates time that mitosis started. Height on the y-axis represents the mitotic duration of that mitosis. The symbol identifies mitotic outcome. (e) Image of DAPI stained HeLa parental cells with a micronucleus identified by an arrow. (f) Quantitation of the percentage of cells containing micronuclei in HeLa parental and HeLa$^{H2B\text{-}2FP}$ cultures (mean ± s.d., n = 3 biological replicates quantifying ≥ 445 nuclei per replicate, *ns* = not significant, student t-test). Scale bars equal 10 μm.

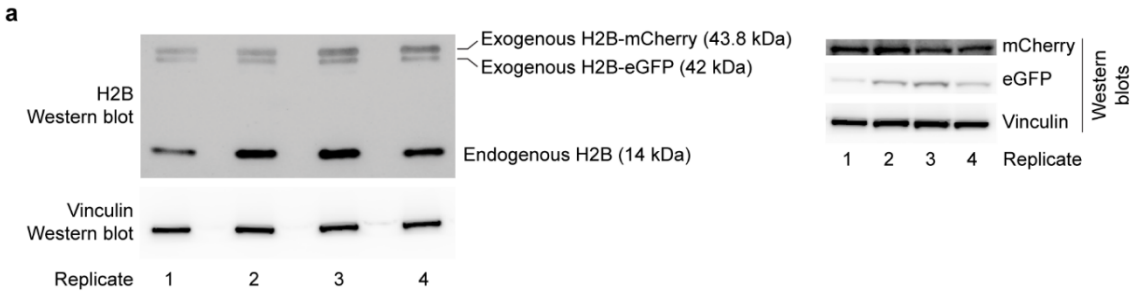

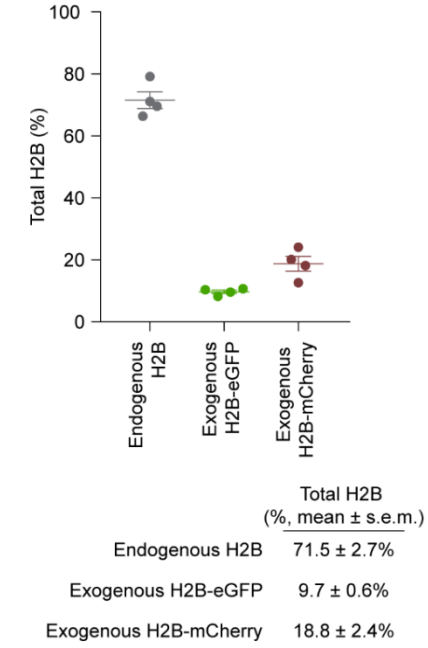

	Total H2B (%, mean ± s.e.m.)
Endogenous H2B	71.5 ± 2.7%
Exogenous H2B-eGFP	9.7 ± 0.6%
Exogenous H2B-mCherry	18.8 ± 2.4%

c

Nucleosomes (%) = [Probability H2B (1) x Probability H2B (2)] x 100

All nucleosome outcomes

H2B (i)	x	H2B (ii)	=	Nucleosomes (%)
Endogenous		Endogenous		51.1%
Endogenous		eGFP		6.94%
Endogenous		mCherry		13.4%
eGFP		Endogenous		6.94%
eGFP		eGFP		0.94%
eGFP		mCherry		1.82%
mCherry		Endogenous		13.4%
mCherry		eGFP		1.82%
mCherry		mCherry		3.53%

Outcomes grouped by included fluorophore(s)

Nucleosomes with no fluorophore	51.1%
Nucleosomes with only eGFP	14.8%
Nucleosomes with only mCherry	30.3%
Nucleosomes with eGFP and mCherry	3.7%

Figure S2: Quantitation of fluorophore tagged H2B abundance in HeLa$^{H2B\text{-}2FP}$. (a) Western blot on four independently collected whole cell extracts from HeLa$^{H2B\text{-}2FP}$ probed for H2B and a loading control (left). Individual H2B species were identified by their predicted molecular weight. Extracts were also separated on additional gels and probed for mCherry or GFP as a control (right). (b) Quantitation of the contribution of each H2B species from the blot in (a) normalized to the respective loading control. (c) Calculation of all possible nucleosome outcomes in HeLa$^{H2B\text{-}2FP}$ from the quantitative data in (b).

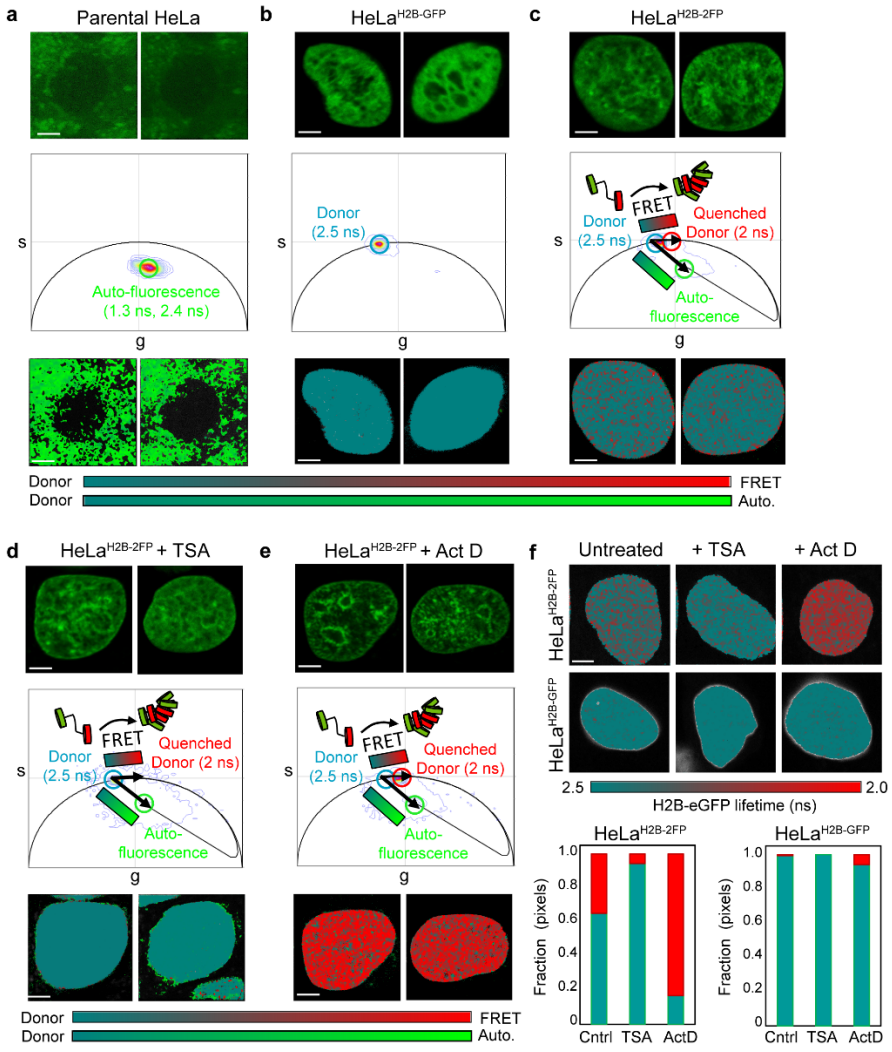

Figure S3: Establishment of background autofluorescence, FRET efficiency, and the phasor location of open versus compacted chromatin in HeLa$^{H2B\text{-}2FP}$. (a) FLIM-FRET analysis of a parental HeLa nucleus to establish the fluorescence lifetime of cellular autofluorescence. (b) FLIM-FRET analysis of a HeLa nucleus expressing only H2B-eGFP (HeLa$^{H2B\text{-}GFP}$) to establish the unquenched fluorescence lifetime and phasor location of H2B-eGFP (0% FRET, starting position of FRET trajectory) ($\tau_{H2B\text{-}eGFP\ unquenched}$ = 2.5 ns). (c) FLIM-FRET analysis of H2B-eGFP in untreated HeLa$^{H2B\text{-}2FP}$ cells. The linear combination of unquenched donor and cellular autofluorescence (teal to green) follow a distinct trajectory from FRET (teal to red). (d) HeLa$^{H2B\text{-}2FP}$ cells treated with TSA to identify the phasor location of open chromatin (0% FRET, $\tau_{H2B\text{-}eGFP}$ = 2.5 ns). (e) HeLa$^{H2B\text{-}2FP}$ cells treated with Actinomycin D (Act D) to identify the phasor location of compact chromatin (21% FRET, $\tau_{H2B\text{-}eGFP}$ = 2.0 ns). (f) Comparison of FLIM-FRET maps derived in HeLa$^{H2B\text{-}2FP}$ (top row) versus HeLa$^{H2B\text{-}GFP}$ (bottom row) after treatment with TSA and Actinomycin D demonstrate the phasor palette defined in (c-e) to report on changes in chromatin network organization specifically due to hetero-FRET. This observation was quantified by counting the fraction of pixels in an open versus compacted chromatin state (HeLa$^{H2B\text{-}2FP}$ N=8 cells, HeLa$^{H2B\text{-}GFP}$ N=3 cells). Scale bars equal 5 μm.

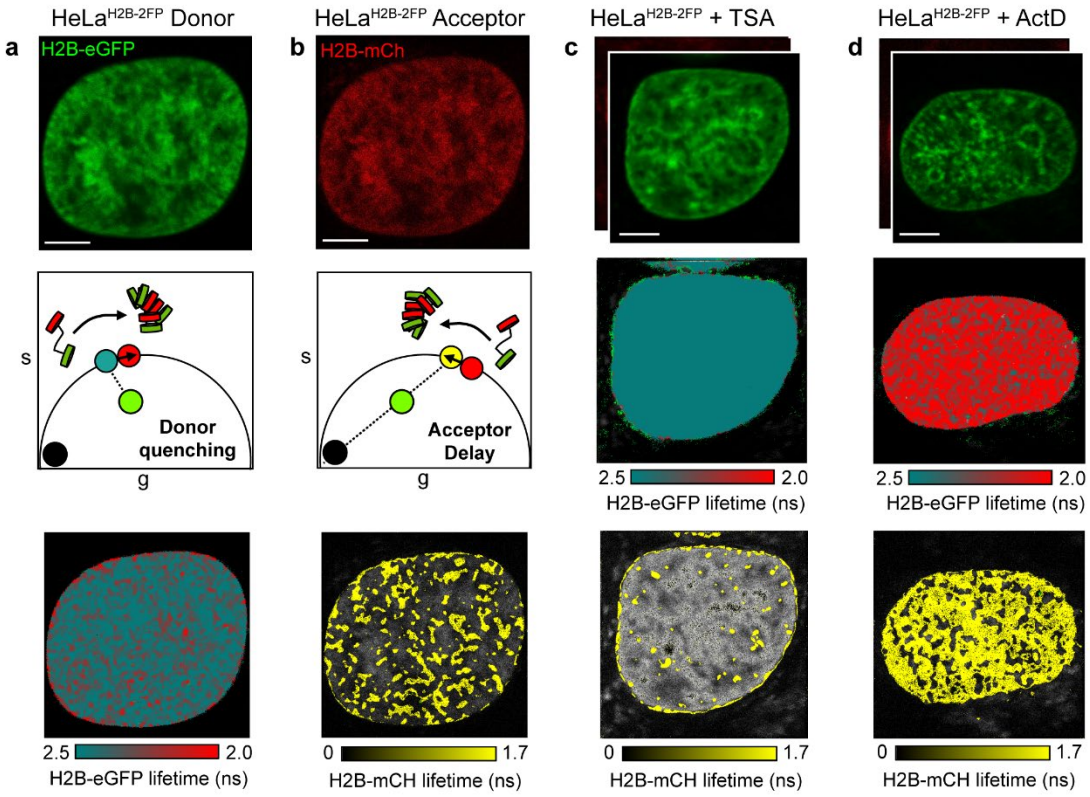

Figure S4: FLIM analysis of the acceptor channel verifies the localization of H2B-eGFP quenched lifetimes detected in the donor channel to be the result of an energy transfer from H2B-eGFP to H2B-mCherry. (a) FLIM-FRET analysis of the untreated HeLa$^{H2B-2FP}$ cell presented in Fig. 1d in the donor channel (H2B-eGFP): pixels undergoing FRET are accurately detected, and the efficiency of energy transfer quantified, from the quenching of the donor lifetime along the universal circle. (b) FLIM-FRET analysis of the HeLa$^{H2B-2FP}$ cell presented in (a) in the acceptor channel (H2B-mCherry): to confirm the localization of FRET observed in the donor channel, we map the localization of delayed acceptor lifetimes in the H2B-mCherry channel using a linked palette which extends from 1.7 ns to the background phasor (0,0). (c)-(d) Comparison of the FRET localization recovered from analysis of H2B-eGFP quenching in the donor channel versus H2B-mCherry delayed lifetimes in the acceptor channel for TSA (c) and Actinomycin D (d) treated HeLa$^{H2B-2FP}$. Scale bars equal 5 μm.

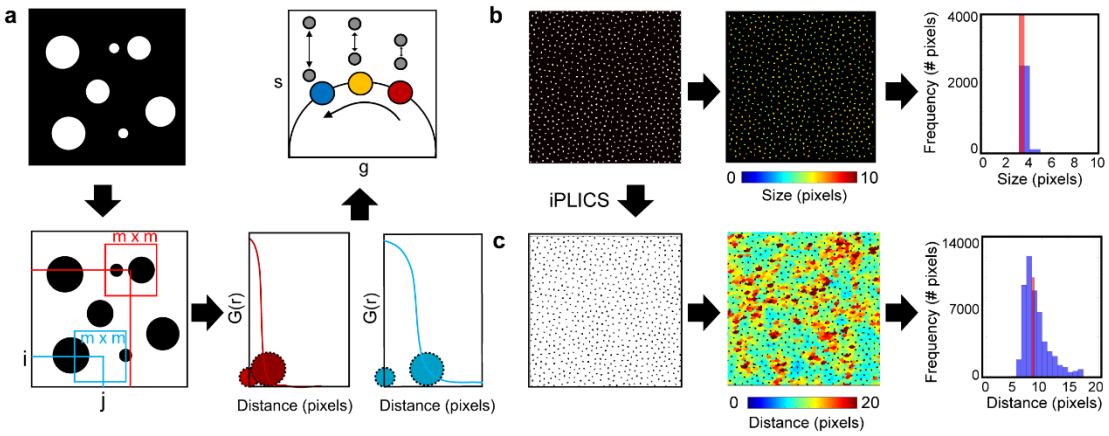

Figure S5: iPLICS analysis and a simulation to demonstrate the feasibility of quantifying chromatin foci size and spacing. (a) Schematic of iPLICS analysis: iPLICS starts with taking the negative of a chromatin localization map, and then analogous to PLICS analysis, calculates localized two-dimensional spatial correlation functions that when collapsed into one-dimensional correlation profiles describe the characteristic spacing between structures within each m x m matrix. Accordingly, by transforming each decay into phasor coordinates (g, s), we can graphically pseudo-color each pixel according to spacing. (b) Simulation of circular binary structures with a diameter of 3 pixels and average distance between them of 8 pixels (left panel) enables derivation of a size map (middle panel) and the histogram of sizes that are pseudo-colored (right panel). (c) Negative image of the simulation described in (b) enables inverse PLICS (iPLICS) analysis and therefore derivation of a distance map (middle panel) and the histogram of distances that are pseudo-colored (right panel).

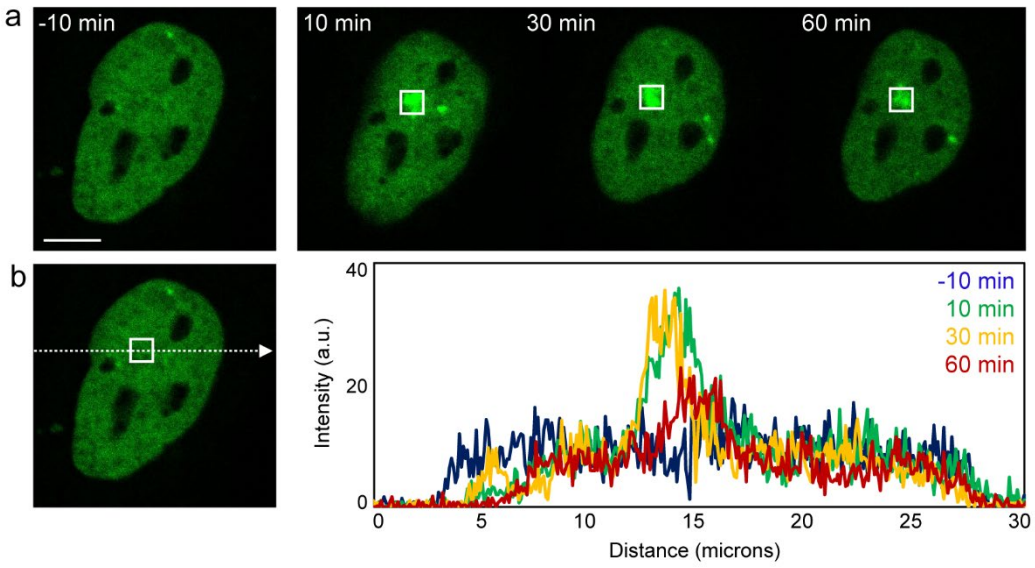

Figure S6: Optimization of NIR laser micro-irradiation conditions to induce double strand breaks. (a) NIR laser micro-irradiation of a HeLa nucleus expressing 53BP1-eGFP with the Ti Sapphire 2-Photon laser operated at 780nm -10 min before and then at different time points during the first hour of the DNA damage response. (b) Intensity along a line scan that traverses the double strand break induced in (a) as a function of time reveals maximum recruitment at 30 min post NIR laser micro-irradiation. Scale bar equals 5 μm.

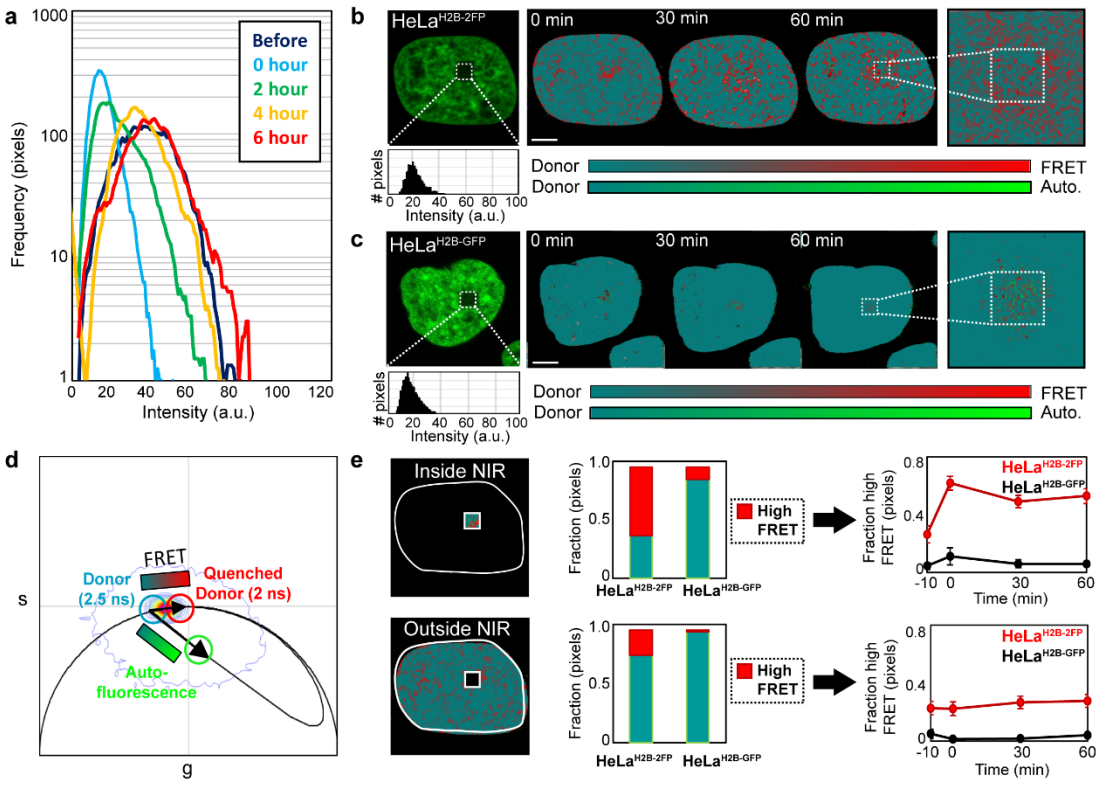

Figure S7: Shortening of H2B-eGFP fluorescence lifetime in HeLa$^{H2B-2FP}$ following NIR laser micro-irradiation results from bona fide hetero-FRET. (a) Histogram of pixels intensities inside the NIR laser micro-irradiation site of Fig. 3c at 2 h intervals. (b) Intensity image of the HeLa$^{H2B-2FP}$ cell presented in Fig. 3 0 min after NIR laser micro-irradiation, with the histogram of pixel intensities inside the DNA damage site (left hand panel), and the corresponding FLIM-FRET maps at 30 min intervals during the following hour, with a digital enlargement of the NIR laser treated ROI shown at 60 min (right hand panels). (c) Intensity image of a HeLa$^{H2B-GFP}$ cell 0 min after NIR laser micro-irradiation, with the histogram of pixel intensities inside the DNA damage site (left hand panel), and the corresponding FLIM-FRET maps at 30 min intervals during the following hour, with a digital enlargement of the NIR laser treated ROI shown at 60 min (right hand panels). (d) Palette employed to pseudo-color phasor FLIM FRET maps presented in (b, c): (1) teal to green highlights the linear combination of unquenched donor and cellular autofluorescence (i.e. trajectory of photobleaching) and (2) teal to red highlights the quenching of the donor lifetime upon FRET interaction. (e) Quantitation of the fraction of high FRET pixels in the DNA damage site versus outside this ROI in HeLa$^{H2B-2FP}$ versus HeLa$^{H2B-GFP}$ demonstrate that the increased FRET signal detected in Fig. 3e in response to DSB induction occurs specifically due to bona fide hetero-FRET, our readout of chromatin compaction (N=10 HeLa$^{H2B-2FP}$ and N=3 HeLa$^{H2B-GFP}$, mean ± s.e.m.). Scale bars equal 5 µm.

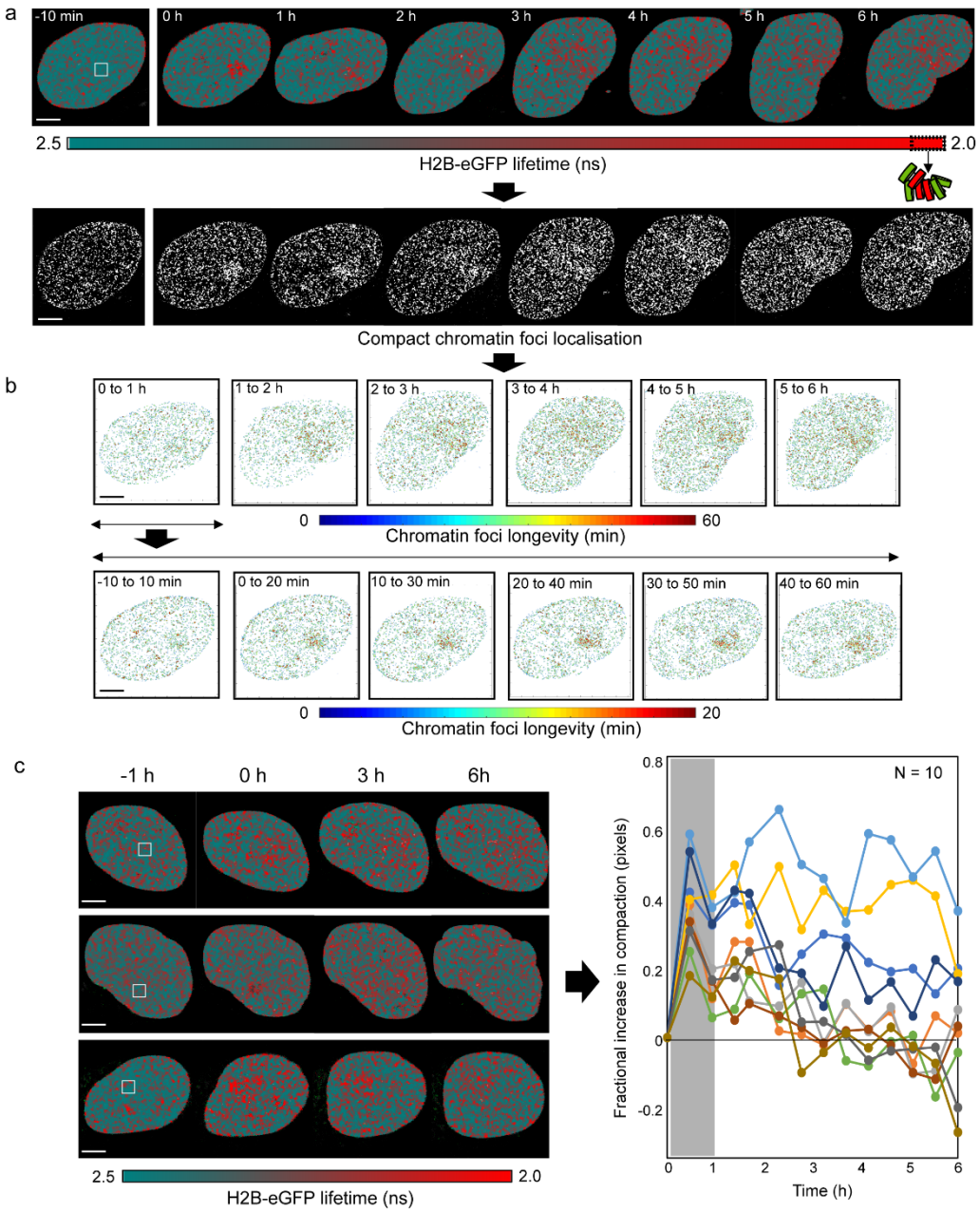

Figure S8: Heterogeneous resolution of the chromatin architecture after NIR irradiation. (a) FLIM-FRET maps acquired in a HeLa$^{H2B\text{-}2FP}$ cell (the same cell is presented in Fig. 6a) 10 min before and for 6 h after NIR irradiation (above) and their corresponding derived compact chromatin localization maps (below). (b) Longevity analysis of the full time series of compact chromatin localization maps from (a) centered at every hour (top row) or every ten minutes for the first hour (bottom row). (c) Left: Phasor maps from three examples of HeLa$^{H2B\text{-}2FP}$ nuclei following NIR laser irradiation. Right: quantitation of the fractional increase in compact chromatin across ten HeLa$^{H2B\text{-}2FP}$ cells following NIR laser irradiation. The grey boxes identify homogenous establishment of chromatin architecture following DSB induction, prior to the heterogenous resolution. Scale bars equal 5 µm.

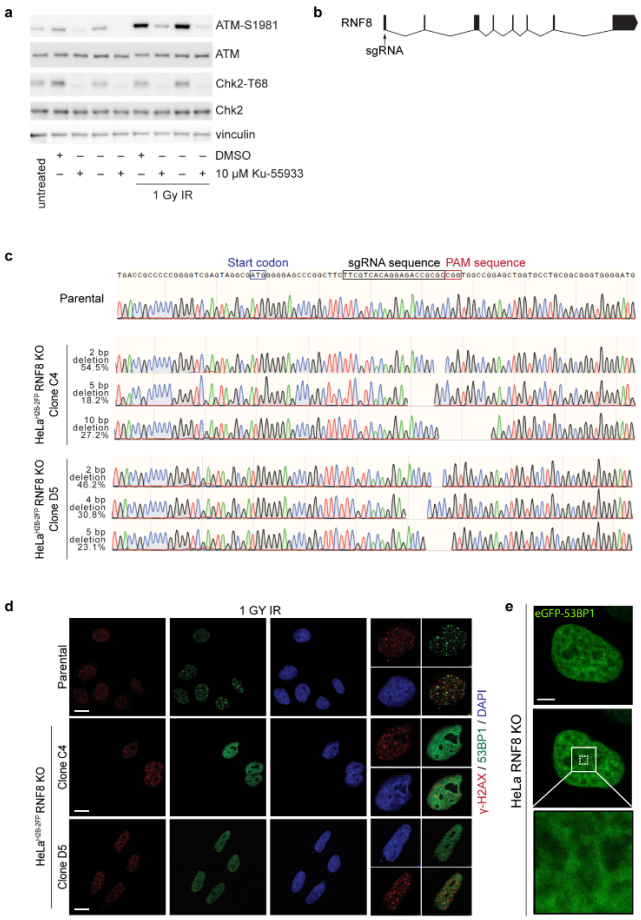

Figure S9: Verification of ATM inhibition and RNF8 knockout HeLa$^{H2B\text{-}2FP}$. (a) Western blots of whole cell extracts from HeLa$^{H2B\text{-}2FP}$ cultures treated with vehicle (DMSO) or KU-55933, ± 1 Gray ionizing radiation (1 GY IR). (b) Gene architecture of RNF8 and targeting of exon 1 by CRISPR/Cas9. c) Sequencing data of HeLa parental and CRISPR/Cas9 generated HeLa$^{H2B\text{-}2FP}$ RNF8 KO clones. The start codon, targeting sgRNA, and PAM sequence are shown. HeLa cells contain three alleles of RNF8. HeLa$^{H2B\text{-}2FP}$ RNF8 KO Clone C4 contained frame shifts inducing deletions of 2, 5 or 10 basepairs, while Clone D5 contained frameshift inducing deletions of 2, 4 and 5 basepairs. In order to resolve the genotype of mixed indel populations, a region surrounding the sgRNA targeted site was PCR amplified, subcloned into pcDNA3.1 and transformed into E.coli. 11 and 9 individual clones were sequenced for Clone C4 and D5 respectively. The percentage of clones with each targeted sequence are shown to the left of the sequencing traces. (d) Immunofluorescence verification of RNF8 knockout. RNF8 is essential for 53BP1 recruitment to γ-H2AX-labelled double strand breaks induced by IR. HeLa$^{H2B\text{-}2FP}$, and HeLa$^{H2B\text{-}2FP}$ RNF8 KO Clones C4 and D5 were treated with 1 GY IR, fixed and stained for γ-H2AX and 53BP1. 53BP1 localization to γ-H2AX foci is evident in HeLa$^{H2B\text{-}2FP}$ but not the RNF8 KO clones. H2B-mCherry and H2B-eGFP are expressed at low levels enabling visualization of the strong γ-H2AX and 53BP1 IF staining following irradiation. Scale bar Scale bar equals 20 μm. (e) Laser micro-irradiation of a HeLa RNF8 KO nucleus expressing 53BP1-eGFP 30 min after NIR treatment using the same conditions identified in Supplementary Figure 6. Scale bar equals 5 μm.

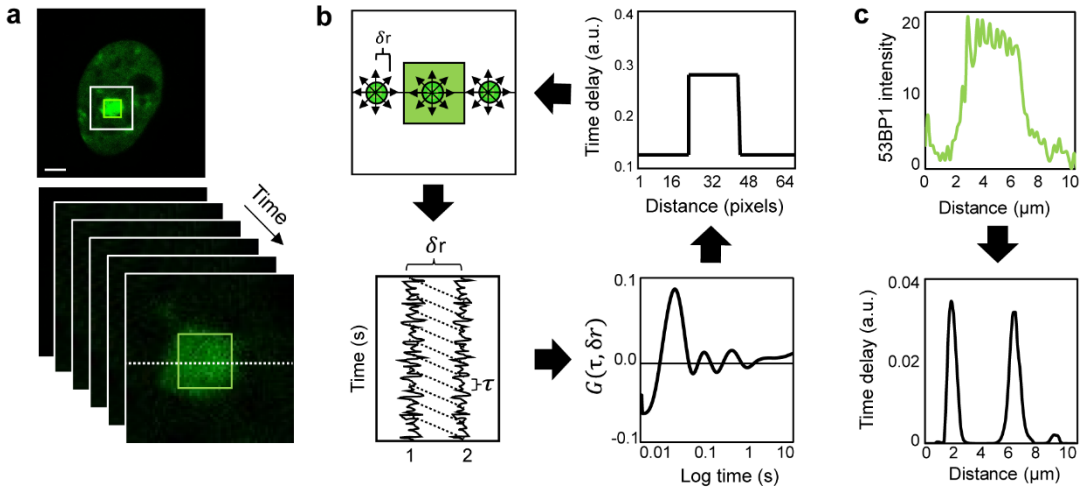

Figure S10: Pair correlation analysis of eGFP-53BP1 mobility. (a) eGFP-53BP1 intensity image acquired in a HeLa cell 30 min after micro-irradiation (top panel, scale bar equals 2 μm) and the region of interest (white box) sampled as a function of time for pair correlation analysis of eGFP-53BP1 mobility (bottom panels). Green box represents the micro-irradiation site and the white dashed line represents a line that pair correlation analysis is performed across in two-dimensions (2D-pCF). (b) Schematic of 2D pCF analysis of eGFP-53BP1 mobility along a line scan that traverses the laser micro-irradiation site: the intensity fluctuation recorded in each pixel along a selected line is radially cross correlated with the intensity fluctuations δr pixels away (top left panel). In each case, a pair of fluorescence intensity fluctuations (1 and 2) are cross correlated for all possible time delays (τ) (left bottom panel) and this operation gives rise to a pair correlation profile that describes the average arrival time of the fluorescent molecules moving between the two locations (bottom right panel). In each pixel position, because we apply the pair correlation function radially, we derive a 2D pCF surface that describes the average time delay of the fluorescent molecules moving away from this location. If we plot this time delay as a function of pixel position along the selected line, we obtain a trace of eGFP mobility (top right panel). (c) When we apply the workflow of analysis described in (b) to the data presented in (a) we are able to correlate eGFP-53BP1 localization (top panel) with eGFP-53BP1 mobility (bottom panel).

Table S1: Oligonucleotides used in this study.

Name	Sequence
BamHI H2B-eGFP forward	5'-GGCGCCGGCCGGATCCATGCCAGAGCCAGCG-3'
EcoRI H2B-eGFP reverse	5'-CTGTGCTGGCGAATTCTTACTTGTACAGCTCGTCCATGCC-3'
sgRNF8-2 sense	5- AAAGGACGAAACACCGGAGCCCGGCTTCTTCGTCACGTTTTAGAGCTAGAA-3'
sgRNF8-2 antisense	5' TTCTAGCTCTAAAACGTGACGAAGAAGCCGGGCTCCGGTGTTTCGTCCTTT-3'
RNF8 exon 1 infusion forward	5'- AGCTGGCTAGCGTTTGGCGATTGCTTCTGTCT-3'
RNF8 exon 1 infusion reverse	5'- CTGATCAGCGGGTTTACCGCTTTCTCCCTTCTCTCC-3'
RNF8 exon 1 sequence	5'- GGCGATTGCTTCTGTCTGTT-3'